DIRECT SIMULATION OF TRAILING-EDGE NOISE GENERATED BY A CONTROLLED DIFFUSION AIRFOIL USING A LATTICE-BOLTZMANN METHOD

M. Sanjosé, S. Moreau
Department of Mechanical Engineering
Université de Sherbrooke
SHERBROOKE, J1K1T1, QC, CANADA
marlene.sanjose@gmail.com

M-S. Kim, F. Pérot
Exa Corporation
Brisbane, CA 94005, USA
perot@exa.com

ABSTRACT

Broadband noise produced by the trailing-edge of a controlled diffusion (CD) airfoil is directly simulated using a Lattice-Boltzmann method (PowerFlow) which resolves both the aerodynamic and acoustic field around the airfoil. A proper DNS resolution is achieved in the vicinity of the airfoil for quasi-2D slice of the mock-up. Two numerical setups of the anechoic open-jet facility where both aerodynamic and acoustic data have been collected are investigated to capture the installation effects: in a first numerical setup (called *free*), the CD airfoil is set in an uniform flow, while in the second setup (*lips*) the real jet nozzle geometry is considered. While in the free-field configuration the boundary layer rapidly detaches on the suction side, in the *lips* the jet shear layers modify the pressure load on the airfoil and the boundary layer keeps attached in the configuration with nozzle. In both setups a laminar recirculation bubble is captured on the suction side near the leading edge. At the reattachment point vortices are emitted and convected either in the wake for the detached flow or along the suction side for the *lips* setup. The wall-pressure and noise spectra for the *free* configuration are spread over a large band of frequencies and agree with similar experimental records at higher angle of attack for which the flow is detached. The spectra for the *lips* configuration better agree with the experimental record, despite a shift to low frequency caused by a lack of stretching due to the limited span-wise extent.

INTRODUCTION

Recent improvements have lead to a strong reduction of tonal noise in rotating machines. Broadband noise contribution is then becoming more and more important. One of the main broadband noise source is the sound produced at the trailing edge of blades. Incoming turbulence or flow disturbance on any lifting surface generates pressure fluctuations and vorticity distortions that diffract on the trailing edge and produce acoustic waves.

Many numerical studies have tried to analyze the flow around airfoils to isolate the trailing-edge (TE) noise mechanisms. In the present study the flow around a controlled diffusion (CD) airfoil in an anechoic open-jet facility is investigated (Fig. 1). The chord based Reynolds number of the configuration is 1.5×10^5 and the Mach number is 0.05, characteristic of low speed fan systems. This configuration has become an excellent study case for trailing edge noise as both aerodynamic and acoustic data have been collected experimentally. The database provides hot-wire measurements to characterize the incoming flow, the boundary-layer on the suction side, near and far wake and the nozzle shear layers (Moreau *et al.*, 2006*a*; Neal, 2010). Mean-pressure coefficient and wall-pressure spectra at several locations on the airfoil pressure and suction sides have also been measured (Roger & Moreau, 2004; Moreau & Roger, 2005). Far field sound and directivities spectra have been recorded in the mid-span plane of the mock-up. Because of the high Reynolds number and the low Mach number, a compressible unsteady simulation to capture the trailing-edge noise source is a daunting task. Previous work (Moreau *et al.*, 2006*b*; Wang *et al.*, 2009) used hybrid methods: a RANS simulation is applied on the full wind tunnel configuration, which provide boundary and initial conditions to an incompressible Large Eddy Simulation (LES) on a restricted domain embedded in the potential core of the open jet. The unsteady wall pressure fluctuations feed acoustic analogies to evaluate the noise prediction from the numerical results but some discrepancies, especially at high frequencies, have been observed between the different analogies. The present study is therefore the first attempt at computing the trailing edge noise on the CD airfoil directly, using a Lattice Boltzmann method. This numerical method is discussed in the next section, numerical set-ups are then described. Aerodynamic and acoustic results are analyzed.

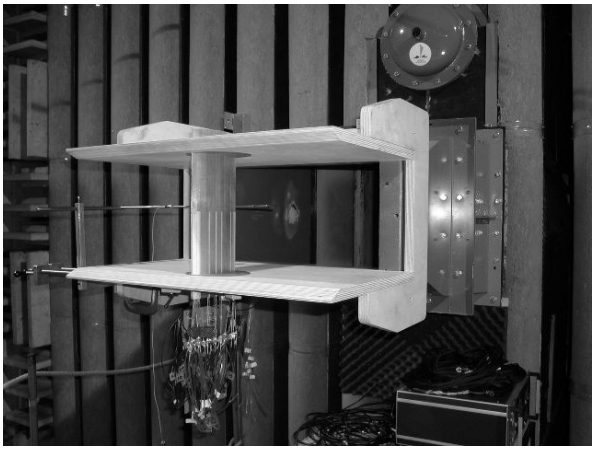

Figure 1. Experimental set-up showing an instrumented airfoil in the ECL anechoic open-jet facility.

LATTICE-BOLTZMANN METHOD

In the present study the Lattice-Boltzmann method (LBM) (He & Luo, 1997; Chen *et al.*, 2006) is applied to the CD airfoil configuration to capture the trailing-edge (TE) noise mechanism. Properties of LBM has been evaluated for acoustics propagation (Brès *et al.*, 2009; Marié *et al.*, 2009). In the present work the Powerflow solver (4.2c) is used, which has been successfully applied to aeroacoustics problems at similar Reynolds number (Brès *et al.*, 2010). The LBM offers significant advantages in terms of integration time and scalability due to a simpler partial differential equations system compared to traditional Navier-Stokes methods.

Instead of studying macroscopic fluid quantities, the LBM tracks the time and space evolution on a lattice grid of a discrete particle distribution function $F_i(\mathbf{x},t)$ which is the mass per unit volume of the particles at time t at the position $\mathbf{x}$ and with velocity c_i. The Lattice-Boltzmann advection equation reads:

$$F_i(\mathbf{x}+\mathbf{c_i}\Delta t, t+\Delta t) - F_i(\mathbf{x},t) = -\frac{1}{\tau}\left(F_i(\mathbf{x},t) - F_i^{eq}(\mathbf{x},t)\right) \tag{1}$$

where the right hand term is the so-called collision operator, approximated by the BGK model. This term drives the particle distribution to the equilibrium with a relaxation time τ.

The discrete Lattice-Boltzmann equations needs to be solved for a finite number of velocity c_i. The discretization retained in Powerflow involves 19 discrete velocities in three dimensions (D3Q19) which has been shown sufficient to recover the Navier-Stokes equations for a perfect gas at low Mach number in isothermal conditions (Frisch *et al.*, 1987).

The equilibrium distribution is approximated by a 2^{nd} order expansion valid for small Mach number (Chen & Dooler, 1998):

$$F_i^{eq} = \rho\omega_i\left[1 + \frac{\mathbf{c_i}\cdot\mathbf{u}}{c_s^2} + \frac{(\mathbf{c_i}\cdot\mathbf{u})^2}{2c_s^4} - \frac{|\mathbf{u}|^2}{2c_s^2}\right] \tag{2}$$

where ω_i are weight function related to the velocity discretization model (Chen & Dooler, 1998; Kotapati *et al.*, 2009). The equilibrium function is related to the macroscopic quantities ρ, $\mathbf{u}$ which can be computed by summing the discrete momentums of the particle distribution.

In Powerflow, a single relaxation time is used, which is related to the dimensionless kinematic viscosity:

$$\nu = c_s^2\left(\tau - \frac{\Delta t}{2}\right) \tag{3}$$

where $c_s = \frac{1}{\sqrt{3}}$ is the dimensionless speed of sound.

The LBM is naturally transient and compressible leading to a direct insight on aerodynamics mechanisms responsible for TE noise sources.

NUMERICAL SETUPS

As shown in (Moreau *et al.*, 2003), the open-jet facility has a major effect on the flow around the airfoil. In the present study, installation effects will further be investigated to evaluate their influence on TE noise sources and propagation.

The two open-jet facility geometries considered in the present study are sketched in Fig. 2, they mimic an horizontal plane of the mockup presented in Fig. 1. In set-up *free*, the airfoil is placed in an uniform flow. The effective width of the jet is neglected, while in set-up *lips* the real thickness of the nozzle throat is considered, and a slight co-flow is added to model air entrainment by the jet. In set-up *lips*, the airfoil is located in the potential core of the open-jet.

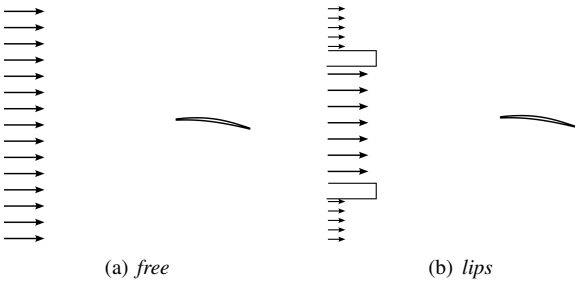

(a) *free* (b) *lips*

Figure 2. Open-jet facility models used in the present study.

The airfoil of chord length C =0.1356 m is located in the middle of the air stream with an incidence of 8°. The operating conditions are given in Tab. 1. The axial and vertical position reference is located at the trailing edge position.

Ambient pressure	P_∞ =101325 Pa
Ambient temperature	T=289 K
Ambient density	ρ_∞ =1.22 kg/s
Uniform/jet velocity	U_{ref} =16 m/s
Coflow velocity	1% U_{ref}

Table 1. Operating conditions of the experimental tests.

In a previous study using the LBM on this configuration, Moreau *et al.* (2004) have highlighted the need for a fine discretization at the surface of the airfoil to correctly capture the laminar-to-turbulence transition of the boundary layer triggered by an unsteady laminar recirculation bubble which appears at the leading edge on the suction side of the CD airfoil (Wang *et al.*, 2009) and prevent a massive flow separation at the trailing edge (observed for "LB-DNS" in Fig. 4 (left) in Moreau *et al.* (2004)). In the present study a DNS resolution has been achieved in the airfoil vicinity.

The configuration is presented in Fig. 3. To reproduce the behavior of the anechoic walls the air viscosity is artificially increased around inlet and outlet boundary conditions, to dump any spurious wave reflections. The mesh is only composed of cubic elements, called *voxels*, whose size is controlled by 10 stacked refinement volumes represented by the grey lines in Fig. 3. The *voxel* size is increased by a factor 2 from one refinement volume to another, insuring a proper flux discretization at the interfaces (Chen *et al.*, 2006), from 15 μm at the airfoil surface to 8 mm at the outlet. Both *free* and *lips* set-ups use identical grid refinement.

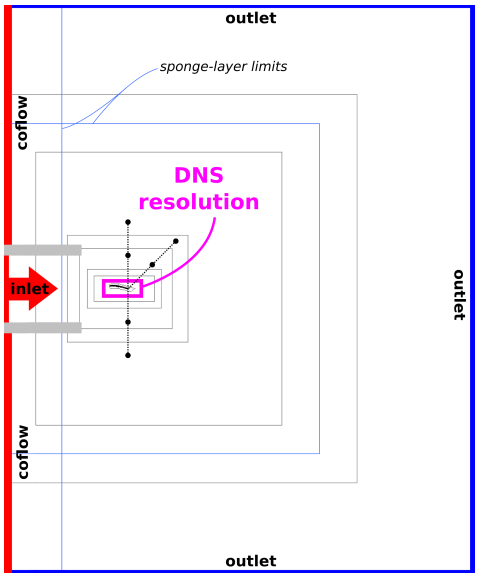

Figure 3. Numerical configuration for the *lips* set-up. The grey lines represent the bounding boxes of the refinement volumes. The black points show probes where pressure fluctuations have been recorded for acoustic study.

The experimental Mach number is about 0.05, but in the simulation, the Mach number has been increased up to 0.2, in order to obtained a proper DNS resolution in the first 3 refinement volume (VR). While computing the dimensionless lattice values, the velocity is increased (by a factor 4) while keeping the sound of speed and the Reynolds number constant, that is by increasing viscosity. In order to prevent numerical instabilities when solving Eq. (1), the relaxation time is kept above a critical value in Powerflow, increasing artificially the fluid viscosity according to Eq. (3). With a higher Mach number, we can ensure that the real viscosity is achieved in the first 3 VR, while it is higher in VR further away with lower mesh resolution.

The present numerical set-ups are quasi-two dimensional, as there is only two layers of *voxels* in the span-wise direction, and a periodicity condition. The final mesh size is about 42 millions of voxels. No turbulent model were used in the present study and a no-slip boundary condition was specified at the airfoil surface in order to precisely capture the laminar to turbulent transition of the boundary layer on the suction side. The simulations were run for 1 s of physical time to reach a stabilized loading on the airfoil and to capture converged statistics.

FLOW AROUND THE AIRFOIL

An instantaneous velocity field around the airfoil in the DNS resolution area is shown in Fig. 4 for the two set-ups. In the *free* set-up the suction side boundary layer is turbulent

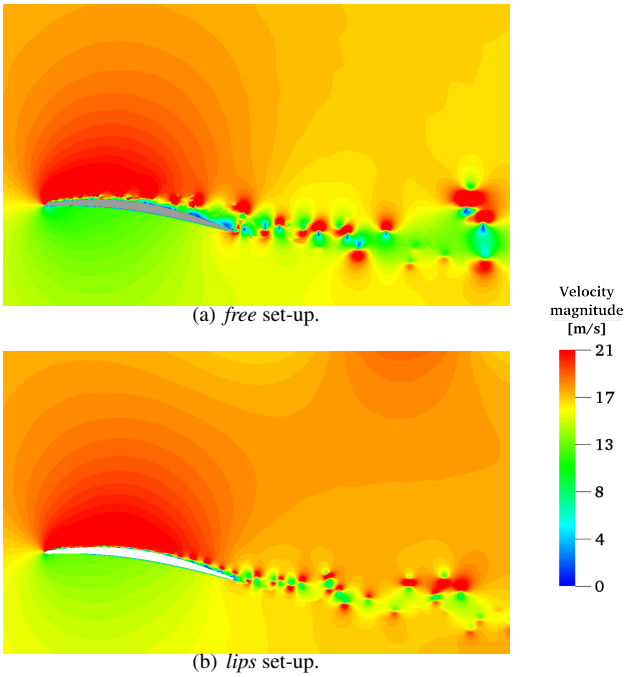

(a) *free* set-up.

(b) *lips* set-up.

Figure 4. Velocity field around the airfoil

starting from the leading edge, and starts to detach at the curvature change. Vortex shedding forms at the trailing edge, caused by the quasi-2D set-up. The vortices stay very coherent, unlike in the experiments at this high Reynolds number. In the *lips* set-up, the suction side boundary layer structure is strongly modified. At the leading edge a laminar detachment appears, at the reattachment point perturbations are generated, which propagates along the suction side. When the curvature changes, these perturbations increase in size and once again stay very coherent due to lack of stretching and dissipation in the span-wise direction. A snapshots in Fig. 5 provide a more precise look at the recirculation bubble. In the *free* set-up, a detachment appear right after the stagnation point. The recirculation quickly destabilizes and generates large vorticity

structures. In the *lips* set-up, the bubble forms progressively and extends three times more in the stream direction. The bubble destabilizes and ejects vortical structure half size of the previous one. By closely comparing the contours in Fig. 5 between the two set-ups, the stagnation point is more on the pressure side in the *free* set-up than in the *lips* one. The jet confinement modifies the angle of attack, as was experimentally observed on a NACA12 by Brooks *et al.* (1986).

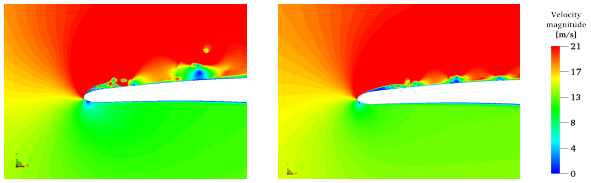

(a) *free* set-up. (b) *lips* set-up.

Figure 5. Velocity field at the leading edge.

SURFACE MEASUREMENTS

The instantaneous pressure has been recorded experimentally using flush-mounted remote microphones (RMP) at mid-span location of the mock-up. Positions are shown in Fig. 6. Boundary layer profiles have been recorded using hot-wire measurement at the same location on the suction side. Only the sensors used in the present study are highlighted with numbers.

Figure 6. RMP locations on the CD airfoil.

The mean wall pressure coefficient is compared to experimental measurements in Fig. 7. It is defined as:

$$C_p = \frac{\overline{p} - p_{\text{ref}}}{\frac{1}{2}\rho_{\text{ref}} U_{\text{ref}}^2} \tag{4}$$

where values indexed with ref are upstream reference values. Without accounting for the real jet width, the pressure distribution along the airfoil can not be captured (Moreau *et al.*, 2003). The *lips* simulation precisely predicts the load on the airfoil surface. At the location of the recirculation bubble, the pressure coefficient shows an increase in suction and a rapid drop at the reattachment point. The phenomenon is strong and short for the *free* set-up compared to the *lips* set-up. Compared to the experimental records, the laminar recirculation bubble in the *lips* simulation seems too large (by a factor of 2) which has already been observed in previous work (Wang *et al.*, 2009).

The boundary layer velocity profiles have been measured with hot-wire (Neal, 2010) in the wall normal direction at the suction side probe location. The same extractions have been done in the mean flow field for both set-ups, the tangential velocity profiles at probe positions 5, 9, 21 and 25 (see Fig. 6)

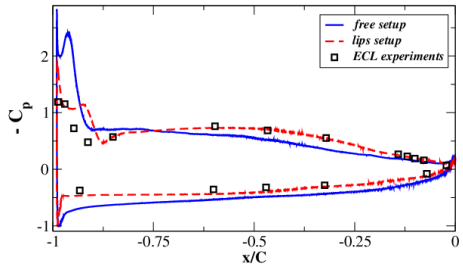

Figure 7. Comparison of pressure coefficient along the airfoil surface for the three set-ups with experimental measurements at ECL on the Large Wind Tunnel.

are given in Fig. 8. The *lips* set-up results provide a very good agreement with the experimental measurements. This highlight that the numerical scheme and the mesh resolution are well suited to correctly resolve the turbulent boundary layer along the suction side. The profiles from the *free* set-up show a very different trend. As observed previously in Fig. 4, the flow is strongly detached at probe location 9, 21 and 25. At probe 5 location both boundary layer profile do not agree with experimental data. The *free* set-up shows a "S" shape, as the lower part of the boundary layer, coming from the reattachment point after the bubble, has a low velocity, and the above part is starting to detach. The boundary layer for the *lips* set-up at probe 5 has the correct shape but is thicker. This profile is taken in the bubble as reverse flow is noticeable, while in the experiments, it has been taken right after the reattachment. Once again, this shows that the predicted recirculation bubble for this simulation is a little too thick and too long.

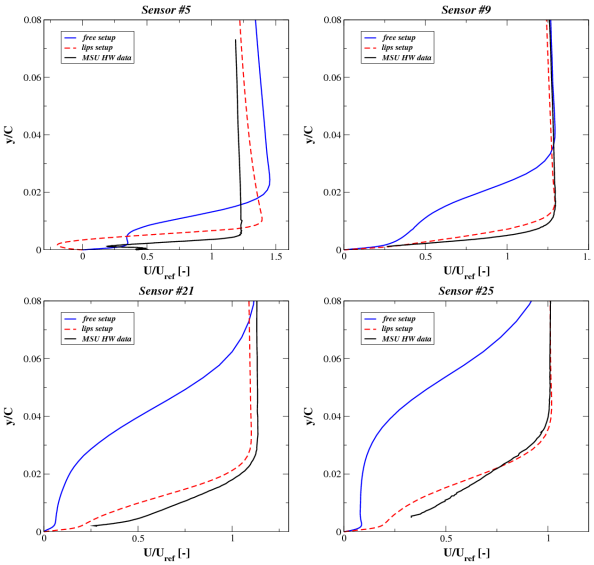

Figure 8. Comparison of boundary layers extracted from mean flow in the two numerical set-ups with experimental measurements.

With the remote microphones, the wall pressure fluctuations have also been recorded. In the present paper, only the

pressure fluctuations at the probe #25 near the trailing-edge are analyzed, as they stand for the noise source in the trailing-edge noise mechanism. The wall pressure spectra $\Phi_{pp}(\omega)$ is made dimensionless using outer parameters of the boundary layer:

$$\Phi^*_{pp}(\omega) = \frac{\Phi_{pp}(\omega)}{\rho^2 \delta^* U_e^3} \tag{5}$$

with δ^* the displacement thickness of the boundary layer, and U_e the outer velocity of the boundary layer.

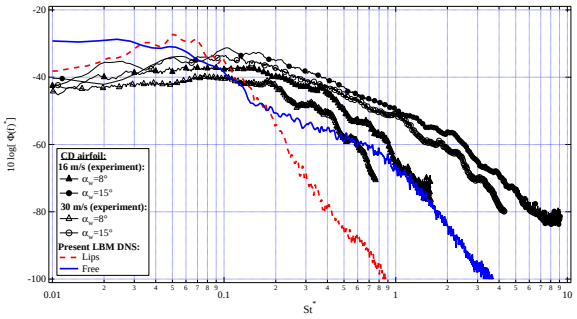

Figure 9. Comparison of normalized wall pressure spectra at probe #25 on the CD airfoil from the *free* and *lips* numerical set-ups with experimental measurements at 8° (present study) and 15° angle of attack.

The normalized spectra is plotted in Fig. 9 as a function of the Strouhal number $St^* = \frac{f\delta^*}{U_e}$ for the present numerical studies, experimental measurements recorded at two angles of attack (8° and 15°) and two jet stream velocity (16 m/s and 30 m/s) on the CD profile. The two numerical set-ups provide very different trends. The *free* spectrum is spreads over a large band of frequency, and has a similar shape than experiments at 15° typical for detached flow. The *lips* spectrum is shifted towards low frequencies compared to experiments at 8°, because of the limited span-wise extent.

ACOUSTIC PROPAGATION

The instantaneous contours of dilatation, $\frac{1}{\rho}\frac{\partial \rho}{\partial t}$, provided in Fig. 10, show the acoustic waves propagation around the airfoil. In the *free* set-up, two major sources can be identified as the divergence point of wave fronts. The first is located at the leading edge of the airfoil and is certainly caused by diffraction of turbulent eddies impacting on the leading edge. The second one is located at the trailing-edge. In the *lips* set-up, the main acoustic source is the TE, which radiates as a dipole source. The waves reflect on the corners of the nozzle lips. As in the NACA12 study of Jones *et al.* (2010), a secondary source appears on the suction side, near the leading edge, at the end of the recirculation bubble.

The noise spectra recorded at 90° and 0.5 m from the trailing-edge is compared to the noise experimentally recorded in the same direction at 2 m from the trailing edge.

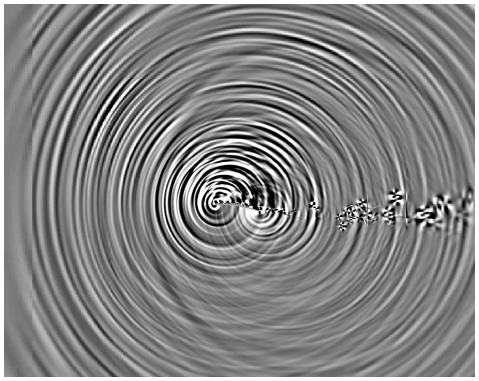

(a) *free* set-up.

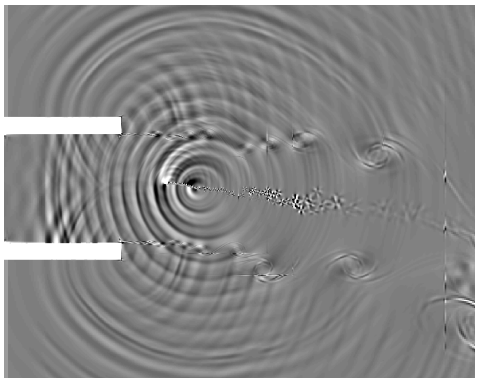

(b) *lips* set-up.

Figure 10. Instantaneous dilatation field in the anechoic chamber. Gray scale from -5 s$^-$1 (black) to 5 s$^-$1 (white).

For the sake of comparisons, the spectra S_{pp} is normalized:

$$S^*_{pp} = S_{pp}\frac{R^2}{U_e^4 l_c} \tag{6}$$

where R is the distance of the microphone to the trailing-edge, and l_c is the coherence length of the sources at the airfoil trailing edge. In the experiments and the previous LES by Wang *et al.* (2009) the coherence length has been estimated to be about $l_c = 3$ mm, while in the present numerical set-ups the coherence length is the span-wise width: $l_c = 30\,\mu$m. The frequency is made dimensionless into a chord based Strouhal number: $St = \frac{fC}{U_e}$.

The normalized acoustic spectra are given in Fig. 11. The numerical simulations provide a noise level of about 10 dB higher than experimental records, and a spectral content more shifted to the low frequencies. This is directly related to the low frequency sources observed in Fig. 9. Nevertheless the shape of the *lips* spectra is similar to the experimental spectrum at 8°, showing that the dipolar radiation is well captured in the present simulation. The secondary source identified in Fig. 10 is responsible for the second pic at St=6. Comparisons with other probes from Fig. 3 show that this source does not propagate towards downstream microphones. The noise spectra from the *free* set-up has a similar shape than the 15° angle of attack noise spectra, typical for a large flow separation on the suction side.

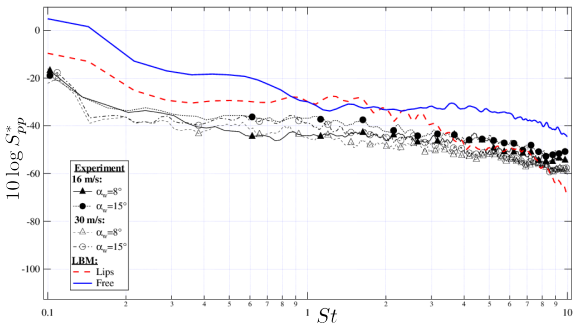

Figure 11. Normalized far field noise spectra at 90° from the trailing-edge.

CONCLUSIONS

In the present study, trailing-edge noise has been numerically investigated on a CD airfoil at 8° angle of attack with a Lattice Boltzmann Method. Two numerical set-ups have been simulated to reproduce the flow and the acoustic propagation around the airfoil in free-field and in an open-jet anechoic facility. The set-ups are quasi-2D and achieve DNS resolution in the airfoil vicinity, which allows to capture the laminar recirculation bubble which occurs near the leading edge on the suction side. The bubble appears short and thick in the *free* set-up which leads to a turbulent boundary layer which quickly detaches. At the leading-edge, the wall pressure spectra looks like the spectra experimentally recorded at higher incidence where the flow is similarly detached. On the contrary the bubble is long and thin in the *lips* set-up, leading to the proper pressure load on the airfoil. The boundary layer is attached up to the leading edge. Instabilities are produced at the bubble reattachment and are convected all along the suction side. The limited span of the numerical set-up keeps these vortices strongly coherent, leading to a wall pressure spectra with a lower frequency content compared to experiments. Nevertheless the *lips* set-up allow to correctly capture the dipolar trailing-edge radiation. The waves diffracts on the nozzle walls modifying the cardioid radiation at high frequency. A secondary acoustic source has been detected in the *lips* set-up, both in the dilatation fields and in the acoustic spectra at 90°. It is generated by the reattachment of the laminar bubble, but is quickly damped compared to the trailing-edge source.

The present study has shown the crucial installation effects on the trailing-edge noise mechanism. The jet shear layers modify the pressure load on the airfoil and the development of the boundary layer on the suction side. The nozzle geometry strongly modifies the acoustic waves propagation also. The 2D limitation of the numerical set-ups has a strong effect on the development of turbulence length scales and on the spectral content of the noise recorded around the airfoil. The first 3D compressible simulation of the CD airfoil configuration is on-going and will probably better agree with experimental measurements.

REFERENCES

Brès, G. A., Pérot, F. & Freed, D. 2009 Properties of the lattice-boltzmann method for acoustics. *AIAA P. 3395* .

Brès, G. A., Wessels, M. & Noelting, S. 2010 Tandem cylinder noise predictions using lattice boltzmann and fowcs williams-hawking methods. *AIAA P. 2010-3791* .

Brooks, T. F., Marcollini, M. A. & Pope, D. S. 1986 Airfoil trailing edge flow measurements. *AIAA J.* **24**, 1245–1251.

Chen, H., Filippova, O., Hoch, J., Molvig, K., Shock, R., Teixeira, C. & Zhang, R. 2006 Grid refinement in lattice boltzmann methods based on volumetric formulation. *Phys. A: Stat. Mech. Appl.* **362** (1), 158–167.

Chen, S. & Dooler, G. D. 1998 Lattice Boltzmann method for fluid flows. *Ann. Rev. Fluid Mech.* **30**, 329–364.

Frisch, U., D'Humiéres, D., Hasslacher, B., Lallemend, P., Pomeau, Y. & Rivet, J-P. 1987 Lattice gas hydrodynamics in two and three dimensions. *Complex Syst.* **1**, 649–707.

He, X. & Luo, L-S. 1997 Theory of the lattice-boltzmann method: From the boltzmann equation to the lattice boltzmann equation. *Phys. Rev. E* **56** (6), 6811–6817.

Jones, L.E., Sandberg, R.D. & Sandham, N.D. 2010 Stability and receptivity characteristics of a laminar separation bubble on an aerofoil. *J. Fluid Mech.* **648**, 257–296.

Kotapati, R., Keating, A., Kandasamy, S., Duncan, B., Shock, R. & Chen, H. 2009 The lattice-boltzmann-vles method for automotive fluid dynamics simulation, a review. In *Symposium in International Automative Technology*. Pune, India.

Marié, S., Ricot, D. & Sagaut, P. 2009 Comparison between lattice Boltzmann method and Navier-Stokes high order schemes for computational aeroacoustics. *J. Comp. Phys.* **228**, 1056–1070.

Moreau, S., Henner, M., Iaccarino, G., Wang, M. & Roger, M. 2003 Analysis of flow conditions in free-jet experiments for studying airfoil self-noise. *AIAA J.* **41** (10), 1895–1905.

Moreau, S., Iaccarino, G., Kang, S., Y., Khaligi & Wang, M. 2004 Numerical simulation of a low speed fan blade. In *Proceedings of the 2004 Summer Program*, pp. 195–207. Center for Turbulence Research, Stanford Univ./NASA Ames.

Moreau, S., Neal, D. & Foss, J. 2006*a* Hot-wire measurements around a controlled diffusion airfoil in an open-jet anechoic wind tunnel. *J. Fluids Eng.* **128** (4), 699–706.

Moreau, S., Neal, D., Khaligi, Y., Wang, M. & Iaccarino, G. 2006*b* Validation of unstructured-mesh les of the trailing-edge flow and noise of a controlled-diffusion airfoil. In *Proceedings of the 2006 Summer Program*, pp. 195–207. Center for Turbulence Research, Stanford Univ./NASA Ames.

Moreau, S. & Roger, M. 2005 Effect of airfoil aerodynamic loading on trailing-edge noise sources. *AIAA J.* **43** (1), 41–52.

Neal, D. 2010 The effects of rotation on the flow field over a controlled-diffusion airfoil. PhD thesis, Michigan State University.

Roger, M. & Moreau, S. 2004 Broadband self noise from loaded fan blades. *AIAA J.* **42** (3), 536–544.

Wang, M., Moreau, S., Iaccarino, G. & Roger, M. 2009 Les prediction of wall-pressure fluctuations and noise of a low-speed airfoil. *Int. J. Aeroacoustics* **8** (3), 177–197.